The Journal of Experimental Biology 211, 1948-1957
Published by The Company of Biologists 2008
doi:10.1242/jeb.014225

The role of proline in the elastic mechanism of hydrated spider silks

Ken N. Savage and John M. Gosline*

Department of Zoology, 6270 University Boulevard, University of British Columbia, Vancouver, British Columbia, Canada, V6K 1Z4

*Author for corresponding (e-mail: gosline@zoology.ubc.ca)

Accepted 5 April 2008

SUMMARY

This study used thermoelastic measurements to investigate the role of proline in the elastic mechanism of hydrated, spider major ampullate (MA) and flagelliform (FL) silks. Experiments on hydrated MA silk from *Araneus diadematus* (proline content 16%) reveal that conformational entropy elasticity accounts for about 90% of the elastic force at small extensions, but entropy elasticity drops to about half by 50% extension. The decrease in the entropic component with extension is due to the presence of relatively short and conformationally restricted network chains in *Araneus* MA silk. Experiments on hydrated *Araneus* FL silk (proline content 16%) indicate that entropy elasticity dominates the elastic mechanism up to extensions of 100% and beyond, which likely reflects the fact that the glycine-rich network chains in FL silk are longer and less conformationally restricted than those in the MA silk. Thus, the rubber-like, entropic elasticity of these two proline-rich silks is consistent with networks of amorphous chains that become mobile when hydrated. By contrast, the elastic mechanism of hydrated *Nephila clavipes* MA silk (proline content 3.5%) shows a small contribution from entropic elasticity for extensions of 5% or less, and by 10% extension the elastic force is due entirely to bond-energy elasticity, probably associated with the deformation of stable secondary structures. These results indicate that there are major differences in the structural organization of the glycine-rich network chains and the mechanism of elasticity in proline-rich and proline-deficient fibroins.

INTRODUCTION

Supercontracted *Araneus diadematus* (Clerck 1757) MA silk exhibits rubber-like, entropic elasticity (Gosline et al., 1984), and this observation provided the basis for the proposal that the fibroin network structure of *Araneus* MA silk contains amorphous network chains that become fully mobile when hydrated. A computer model based on this assumption appears to accurately predict the properties of both dry and hydrated MA silk (Termonia, 1994). In addition, rubber-like elasticity appears to be a suitable model for other hydrated elastomeric proteins such as resilin and elastin (Weis-Fogh, 1961; Dorrington and McCrum, 1977). However, physical characterization of *Nephila clavipes* (Linnaeus 1767) MA silk indicates that the network chains of this silk are not amorphous but contain some axially aligned, stable, secondary structures (Kümmerlen et al., 1996; Thiel et al., 1997; van Beek et al., 2002). Thus, there appears to be a discrepancy between fibroin network models that predict amorphous network chains and studies based on X-ray and NMR that predict stable secondary structure. It is worth noting that the amorphous network models have all been applied to materials that are rich in the amino acid proline, whereas physical studies identifying the presence of secondary structure have been based on *Nephila* silk, which contains little proline.

Sequencing efforts have revealed a domain architecture to MA silk fibroins that resembles a block copolymer. Each fibroin contains multiples of a basic repeat sequence that contains two blocks, a poly-alanine block that is 8–10 amino acids long, followed by a block of 20–30 amino acids that is rich in glycine. Combined with data from a variety of physical studies, a basic MA silk structure is accepted in which the MA fibroin network consists of a 'soft' matrix of glycine-rich network chains that are crosslinked and reinforced by alanine-rich, β-sheet crystals. Although the structure of the poly-alanine crystals is well understood, the structure of the network chains is not so clear.

The poly-alanine, crystal-forming blocks are similar in all the araneoid MA fibroins sequenced thus far, but these fibroins have been grouped as either spidroin-1 or spidroin-2 based largely on differences in types and arrangements of amino acids within the glycine-rich network chains (Gatesy et al., 2001). Perhaps the most striking difference between the two fibroin groups is the absence of proline in spidroin-1 fibroins and the abundance of proline in spidroin-2 fibroins. Since *Nephila* MA silk contains little proline, spidroin-1 is preferentially expressed in the MA glands of *Nephila*. Conversely, *Araneus* MA glands express two spidroin-2 fibroins and contain about 16% proline (Guerette et al., 1996). It is the differential expression of these two fibroin types in *Nephila* and *Araneus* that may explain the differences observed in the structure of the glycine-rich network chains in the MA silks of these spiders. That is, because proline is known to disrupt secondary structures in proteins, differences in proline content may be responsible for the observed differences in the structure of the glycine-rich network chains. Indeed, Rauscher et al. (Rauscher et al., 2006) analysed the proline and glycine levels across a range of elastin-like and amyloidic peptides and found that peptides above a well defined threshold of glycine and proline content form amorphous, highly hydrated and kinetically mobile (i.e. elastin-like) aggregates, whereas peptides falling below the threshold formed amyloid-like structures with significant β-sheet content. For a given level of glycine, there is a threshold level of proline that provides elastomeric properties, but below the threshold a protein is rigid and amyloid-like. Spidroin-1 and spidroin-2 network chains have similar levels of glycine (~45% and 40%, respectively), but they differ strongly in proline content (0% and 15–18%, respectively). As a consequence, the spidroin-2 chains lie well above the threshold, along with the elastomeric proteins elastin, resilin and abductin, whereas is spidroin-1 chains fall below the threshold, along with known amyloidogenic sequences.

The accompanying paper (Savage and Gosline, 2008) clearly documents differences in the mechanical and optical properties of proline-rich *Araneus* MA silk and the proline-deficient *Nephila* MA silk in their hydrated states. That is, *Nephila* MA silk contains a more ordered fibroin network than does *Araneus* MA silk, and when hydrated, *Nephila* silk remains stiffer and more highly birefringent because the network chains retain much of their hydrogen-bonded structure. It was hypothesized that this difference in network structure would mean that *Nephila* and *Araneus* MA silks will exhibit inherently different elastic mechanisms in their hydrated states, and this hypothesis is tested explicitly in the current study. Specifically we test the hypothesis that proline-rich silks will be elastin-like and will exhibit rubber-like elasticity, based on changes in the conformational entropy of kinetically free protein chains with extension, whereas proline-deficient silks will have an elastic mechanism consistent with a crystalline material and hence exhibit bond-energy elasticity.

Unlike the MA silks sequenced so far, the crystal crosslinks in FL silk have not been clearly identified, although sequence data for FL silks from several spider species indicate that FL fibroins also have a block copolymer structure. Each FL fibroin consists of a repeated 'spacer' block and a longer glycine-rich 'network-chain' block (Gatesy et al., 2001). The glycine-rich sequences are similar to those found in the spidroin-2 MA fibroins, but the presumed network chains in FL fibroins are 5–15 times longer than those in MA fibroins. However, the glycine–proline content of FL fibroins is essentially identical to that of the spidroin-2 MA fibroins, which we hypothesize will exhibit conformational entropy elasticity. Thus, we hypothesize that hydrated FL silks will also exhibit conformational entropy elasticity.

In this study we use thermoelastic experiments to test these hypotheses. Our results indicate that proline-rich MA and FL silks from *Araneus diadematus* exhibit rubber-like, conformational-entropy elasticity, although in the MA silk bond-energy elasticity becomes important as extensions approach 50%. The proline-deficient MA silk from *Nephila clavipes* exhibits a small component of entropic elasticity at small extensions, but at 10% extension and above the material shows essentially 100% bond-energy elasticity.

Thermoelasticity

The work done to stretch an elastic body is stored as a change in internal energy (E) and as a change in entropy (S). It as been shown that, at constant temperature (T), volume (V) and composition (n), the retractive force developed when an elastic material is stretched is given as (Flory, 1953; Treloar, 1975):

$$\mathbf{F} = (\partial E/\partial L)_{T,V,n} - T(\partial S/\partial L)_{T,V,n} . \quad (1)$$

The first term on the right, the change in internal energy with length, is due to the deformation of chemical bonds in a rigid, often crystalline, material. The second term, the entropy changes with length, arises from changes in the shape of flexible polymer molecules, such as those found in rubber networks. Note that the entropy term includes temperature because as temperature increases so does the thermal agitation of the network chains. Thus the entropic component of the elastic force increases as temperature increases. It can be shown that $(\partial S/\partial L)_{T,V,n}=-(\partial \mathbf{F}/\partial T)_{L,V,n}$ (Flory, 1953), so that Eqn 1 becomes:

$$\mathbf{F} = (\partial E/\partial \mathrm{L})_{T,V,n} + T(\partial \mathbf{F}/\partial T)_{L,V,n} , \quad (2)$$

and this equation provides the basis for a simple, thermoelastic experiment that can be used to determine the relative contributions of bond-energy and conformational-entropy changes to the elastic mechanism of any material. A sample is stretched and held at fixed length and constant volume, and the force is measured while the temperature is varied. The slope of the resulting force–temperature plot yields the entropic component of the elastic force, $\mathbf{F}_s$. At zero degrees kelvin (0 K), where there is no molecular motion, there is no entropy, and thus the intercept of the force–temperature curve at 0 K yields the internal energy component of the elastic force, $\mathbf{F}_e$.

Rubbery materials are commonly associated with low stiffness and high extensibility, but these attributes do not necessarily classify a material as being a rubber. A rubber must meet two distinguishing criteria: (1) the elastic force in a rubber is due primarily to changes in the conformational entropy of kinetically free polymer chains caused by extension, which means that the force on a rubber at a fixed extension will increase linearly with increasing temperature; (2) the internal energy change associated with bond deformation should contribute to a small fraction of the total force and be nearly constant over a large range of extension and temperature.

However, thermoelastic tests can only be used to determine the changes in conformational entropy and bond-energy if the tests are carried out at constant volume and molar composition, as indicated by the subscripts in Eqn 2. This is because in an open system, there are other processes such as thermal expansion and polymer–solvent mixing that can contribute to changes in entropy and to changes in internal energy. Even in a closed system, where the material cannot absorb solvent, it is not possible in practice, to perform a test at constant volume due to the thermal expansion of the material, and so the material is tested at constant pressure, P, but the force–temperature slope is corrected for thermal expansion by measuring the force at constant extension ratio (λ). The retractive force, $\mathbf{F}$, becomes (Flory, 1953):

$$\mathbf{F} \approx (\partial E/\partial L)_{T,V,n} + T(\partial \mathbf{F}/\partial T)_{\lambda,P,n} . \quad (3)$$

The first term of Eqn 3 gives the bond-energy contribution to the elastic force, $\mathbf{F}_e$, and the second term gives the conformational entropy contribution, $\mathbf{F}_s$. Thus when corrected for thermal expansion, $\mathbf{F}_s \approx \mathbf{F}$, meeting criterion 1, and $\mathbf{F}_e \approx 0$, meeting criterion 2.

Normalizing Eqn 3 to the force, $\mathbf{F}$, yields:

$$\mathbf{F}_e/\mathbf{F} \approx 1 - (T/\mathbf{F})(\partial \mathbf{F}/\partial T)_{\lambda,P,n} . \quad (4)$$

Consequently, the entropic contribution, $\mathbf{F}_s$, is equal to:

$$\mathbf{F}_s/\mathbf{F} = 1 - \mathbf{F}_e/\mathbf{F} . \quad (5)$$

Applying the same criteria to biological materials meets with an added complication. Biological materials act as rubbers only when swollen in a polar solvent such as water (Gosline, 1980). In practice, the swelling effect of water on the sample can vary with temperature, in which case it may not be possible to measure force at either constant volume or constant composition. It is, however, possible to measure force, $\mathbf{F}$ as it varies with temperature, T, at constant length, L, and pressure, P, under equilibrium swelling conditions (eq) (Flory, 1953):

$$\mathbf{F} = (\partial H/\partial L)_{T,P,\mathrm{eq}} + T(\partial \mathbf{F}/\partial T)_{L,P,\mathrm{eq}} . \quad (6)$$

In this case, ∂H is the total enthalpy change of the system, including changes in enthalpy associated with mixing of solvent and network chains. Swelling changes, measured as a function of temperature, can be used to correct $(\partial H/\partial L)_{T,P,\mathrm{eq}}$, giving the bond energy component of elastic force, $(\partial E/\partial L)_{T,V,n}$.

Where swelling changes with temperature are small, $(\partial H/\partial L)_{T,P,\mathrm{eq}} \approx (\partial E/\partial L)_{T,V,n}$ and no correction is required. Both resilin (Weis-Fogh, 1961) and abductin (Alexander, 1966) show small changes in swelling with temperature, and thermoelastic experiments

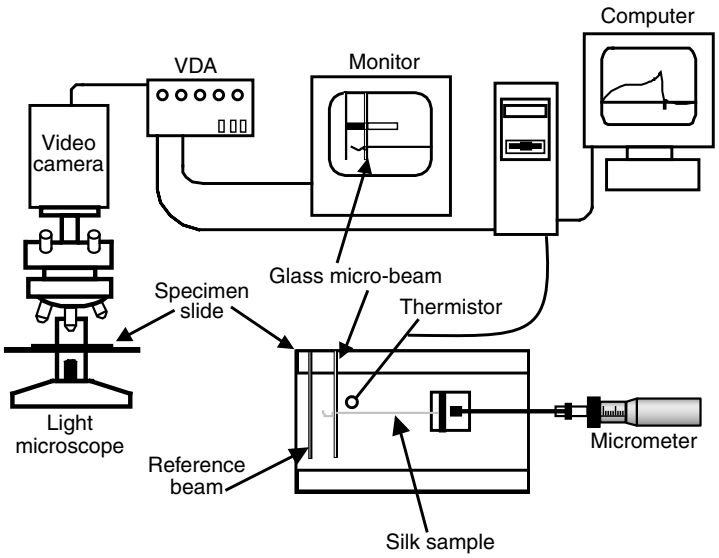

Fig. 1. The micro-beam tensile test apparatus used to measure the thermoelastic properties of spider silks. A supercontracted silk thread (green line) is mounted between a glass beam and a moveable micrometer mount. A video dimension analyzer (VDA) system mounted on a microscope is used to track the deflection of a glass micro-beam relative to a reference glass beam. This provides nano-Newton resolution of changes in the elastic force. A thermistor placed near the silk sample measures temperature.

yields results remarkably similar to those described above for lightly crosslinked rubber. In these cases, $(\partial H/\partial L)_{T,P,\mathrm{eq}}$ is small relative to the entropic component, $(\partial \mathbf{F}/\partial T)_{T,V,n}$. Thus, elastic energy for these two proteins is stored largely as changes in conformational entropy. Water-swollen elastin, however, exhibits very large changes in swelling with temperature, and so $(\partial H/\partial L)_{T,P,\mathrm{eq}} \neq (\partial E/\partial L)_{T,V,n}$ (Gosline, 1980) because there are large enthalpy changes associated with changes in solvent–polymer interactions. When the thermoelastic data are corrected for the temperature-dependent swelling, $(\partial E/\partial L)_{T,V,n}$ is close to zero over a 20% range in extension (Dorrington and McCrum, 1977). Thus, elastin also appears to meet the criteria for rubber elasticity. Similar results were obtained with octopus arterial elastomer (Shadwick and Gosline, 1985), and the methods from these two studies have been used in the current thermoelastic analysis of hydrated spider silks, as described below.

MATERIALS AND METHODS

Thermoelasticity

Thermoelastic measurements were taken using a modification of the glass beam apparatus (Fig. 1) described previously (Gosline et al., 1995; Fudge et al., 2003; Savage et al., 2004). For these experiments, a sample chamber was constructed on a large microscope slide (50 mm×75 mm) that was placed on a temperature-controlled stage with similar dimensions. This assembly was mounted onto a 3 mm thick aluminium plate with plastic legs, which provided thermal isolation, and the plate was clamped to the stage of a Wild M-21 microscope at the very outer edge of the microscope stage. Silk samples were mounted in the sample chamber between a glass beam and a moveable micrometer mount, as above, and a second, reference glass beam mounted adjacent to the first was used to help control for vibrations during thermoelastic experiments. In addition, the reference beam could be used to track the thermal expansion of the temperature-control stage and attached chamber. The sample chamber was closed at the top with a large microscope coverslip, which provided an optically flat surface for tracking the deflection of the glass beams.

The silk was stretched and held at a fixed length at the highest temperature for about 10 min to allow the initial force to stabilize. The temperature was lowered and then raised by switching between two temperature controlled water baths, where one bath was set to the lowest temperature and the other to the highest temperature. The temperature shifts occurred over a time interval of less than 10 min. Movement of the glass beam with changing temperature, relative to the reference beam, was tracked with a video dimension analyzer (VDA; Instruments for Physiology & Medicine, San Diego, CA, USA), and this movement was used to track the change in force with changing temperature. Temperature in the test chamber was measured with a calibrated, thermistor bead that was immersed in the water immediately adjacent to the silk sample. VDA and thermistor outputs were recorded by a PC computer. Following the force–temperature experiment, the silk sample was slackened, and the temperature was again lowered and raised. Movement of the reference beam relative to the optical axis of the microscope provided control data that were used to correct for the thermal expansion of the apparatus.

The voltage output from the VDA was plotted against temperature, and linear regressions were computed for the experimental and the control voltage–temperature data. The control regression was subtracted from the experimental regression to produce a regression for the voltage–temperature relationship of the silk sample held at fixed length (Fig. 2). The application of beam theory with the dimensions of the glass beam allowed the calculated voltage–temperature curve to be transformed to yield a force–temperature curve (Fudge et al., 2003). Since extension of the silk sample also deflects the glass beam used to measure the force, a correction for the beam deflection was applied to obtain the constant-length force on the silk sample.

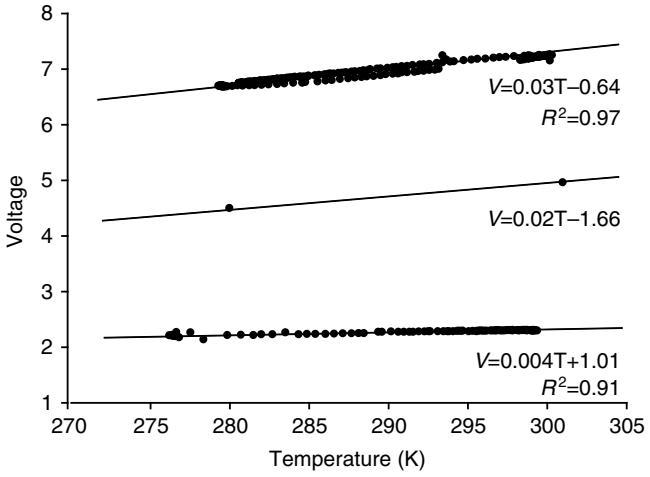

Fig. 2. The raw data from a typical thermoelastic experiment on *Araneus* MA silk. The top curve represents the raw force–temperature data and the bottom curve represents the control data for the expansion of the apparatus. A linear regression fitted to the control data was subtracted from the regression of the raw data to give the corrected voltage-temperature profile of the silk (middle curve).

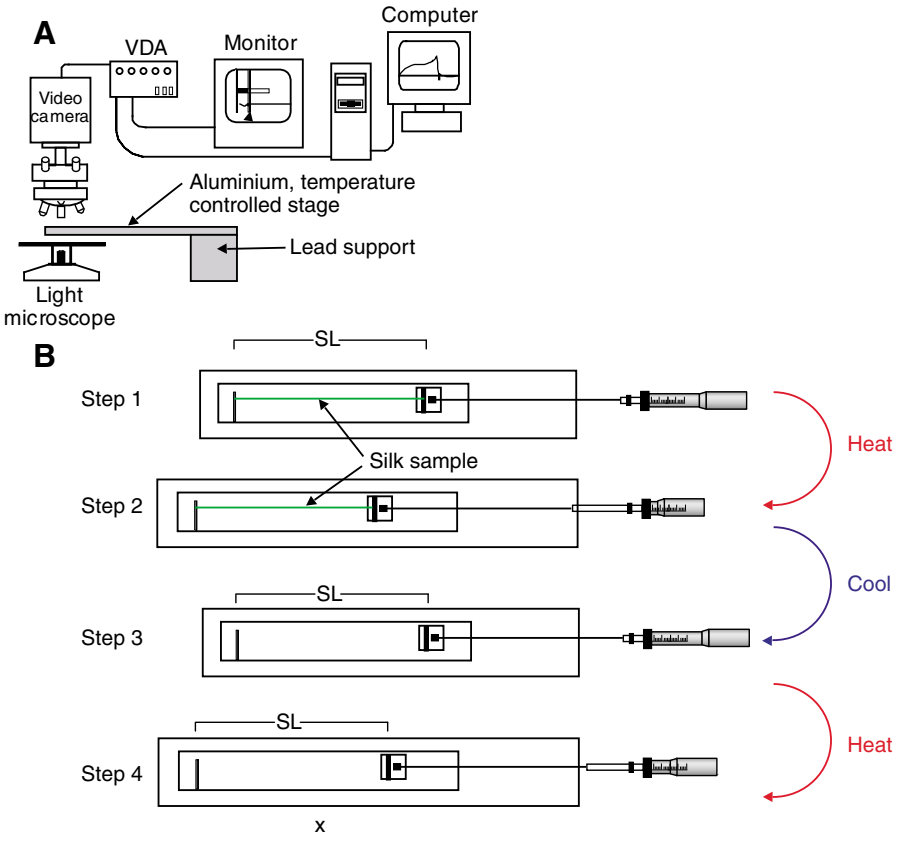

Fig. 3. (A) The micro-beam test apparatus used to measure the thermal swelling coefficients for swollen MA silks. The silk sample is mounted between a glass beam and a moveable micrometer mount in the sample chamber of the aluminium, temperature-controlled stage. The stage was fixed at one end to a lead block located to one side of the microscope, and this assembly was position so that the glass beam was centred in the field of view of the microscope. This setup ensures that the temperature-controlled stage is thermally isolated from the microscope stage, so that movement of the glass beam could be used to track the thermal expansion of the temperature-controlled stage. (B) An expanded view of the temperature-controlled stage with the silk sample chamber, which shows the process for measuring the thermal swelling coefficient of MA silk. In step 1, a silk fibre is mounted in the sample chamber between the glass rod and a moveable micrometer mount, and the initial length, SL, is measured as described in the text. In step 2, the temperature is increased, and a new initial length is measured. The silk sample is then removed and the thermal expansion of the stage was measured by tracking the movement of the unloaded beam over the same temperature range (steps 3 and 4). The movement of the glass beam was subtracted from the calculated length change of the silk with temperature to give the thermal swelling coefficient of the silk.

Extrapolation error

The intercept of the force–temperature profile of the silk at 0 K yields the enthalpy component, $\mathbf{F}_h$, of the elastic force. The error associated with this extrapolation, E_{silk} was calculated from the slope of the raw force–temperature data, S_{silk}, as well as the combined relative errors for the raw force–temperature data and the control data, according to the following equation:

$$E_{\text{silk}} = S_{\text{silk}}\sqrt{\left(\frac{e_{\text{r}}}{s_{\text{r}}}\right)^2 + \left(\frac{e_{\text{c}}}{s_{\text{c}}}\right)^2} \quad . \tag{7}$$

The ratio of the standard error of the slope, e, to the slope, s, was calculated for the force–temperature profile of the experimental data, ($e_{\text{r}}/s_{\text{r}}$) and for the control data ($e_{\text{c}}/s_{\text{c}}$), and these two ratios were then combined in quadrature.

Swelling experiments

The thermal swelling coefficients for swollen MA silks were measured using an aluminium, temperature-controlled stage that contained a sample chamber that was specifically designed to accommodate long silk samples (Fig. 3). MA silk samples were mounted in the sample chamber between a glass beam and a moveable micrometer mount. Water was added to the chamber, and the chamber was covered with a coverslip. The stage was attached at one end to a lead block that was located adjacent to a Wild M-21 polarizing microscope, and this assembly was positioned so that the glass beam at the other end was centred in the field of view of the microscope. The temperature-controlled stage was not directly attached to the microscope stage, so that the movement of the glass beam could be used to track the thermal expansion of the temperature-controlled stage and attached chamber.

A video camera plus VDA were used to track the deflection of the glass beam, which allowed us to determine the force-deflection of the silk sample when it was stretched by the micrometer. Initial lengths of the silk samples were measured with a vernier calliper to 0.1 mm. The change in length with temperature was measured as follows. The temperature of the chamber was set and allowed to equilibrate. The silk was then extended by several percent while tracking the deflection of the glass beam, and the initial length was determined by extrapolating the initial force–extension curve to zero force. This process was repeated four to five times, and an average was taken. The temperature was then raised, and this process was repeated. The length change was calculated as the difference in the micrometer reading for initial length at the two temperatures. This length change was then corrected for the thermal expansion of the stage, which was measured by tracking the movement of the unloaded beam over the same temperature range. That is, the movement of the beam was subtracted from the calculated length change, and this result was divided by the temperature difference to produce the thermal swelling coefficient. The thermal swelling coefficient was assumed to be constant between 283 K and 303 K (Gosline et al., 1984). The silk samples of *Araneus* MA silk were approximately 5.5 cm long, and the *Nephila* MA silk samples were approximately 7 cm long.

RESULTS

In this study thermoelastic experiments were used to reveal the thermodynamic origins of the elastic mechanism in hydrated spider silks to determine if the presence or absence of proline in their network chains causes major shifts in the elastic mechanism. Specifically, we hypothesized that the network chains in the proline-rich fibroins of *Araneus* MA and FL silks are amorphous, and when hydrated these chains become kinetically free random-coils that

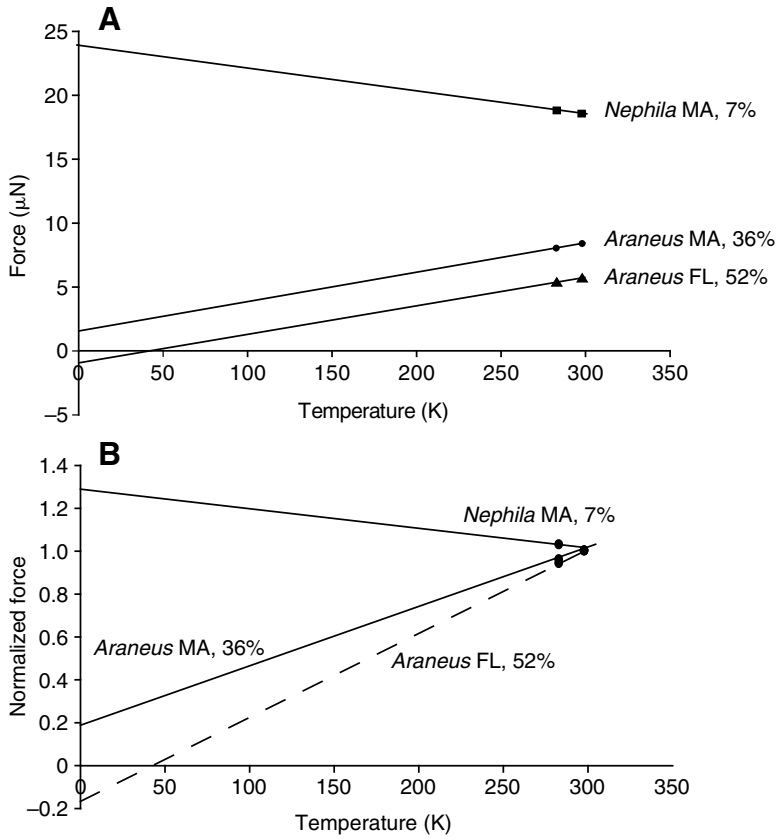

Fig. 4. (A) Typical force–temperature curves, uncorrected for swelling, for *Araneus* and *Nephila* MA silk and *Araneus* FL silk. Each curve consists of two points taken from the linear regression of the raw force data curves. Each curve is labeled for the type of silk and the extension at which the test was administered. (B) The force–temperature curves from Fig. 2 re-plotted as normalized force *vs* temperature. The regressions plotted in Fig. 2 from experimental force–temperature profiles are normalized to the force at 303 K. Each curve is labeled for the type of silk and the extension at which the test was administered.

exhibit rubber-like or entropic elasticity. *Nephila* MA silk contains proline-deficient fibroins, and the relative lack of proline allows their network chains to take on semi-ordered conformations. We hypothesized that these semi-ordered structures will remain stable when this silk is hydrated, and thus that the hydrated silk will exhibit bond-energy elasticity associated with the deformation of these structures. These hypotheses were tested in thermoelastic experiments, as follows.

Force–temperature experiments

Fig. 4A shows the force required to hold a sample of the three silks at a fixed length as temperature is changed between 10 and 30°C. Note that *Nephila* MA silk exhibits a totally different behaviour than the two proline-rich *Araneus* silks. That is, the force–temperature plot for *Nephila* MA silk has a negative slope, and the force–temperature plots for the two *Araneus* silks have positive slopes. It is convenient to normalize the force to a reference temperature, in this case 303 K, as in Fig. 4B, and the intercept of this plot at 0 K, $(\partial H/\partial L)_{T,P,\mathrm{eq}}$, then represents the fraction of total force due to enthalpic changes, $\mathbf{F}_h/\mathbf{F}$, at the reference temperature. The force–temperature plot of this *Nephila* MA silk sample had an intercept of about 1.3, indicating that enthalpic changes are responsible for more than 100% of the total elastic force. The *Araneus* MA force–temperature profile has an intercept of about 0.2, indicating that for this sample approximately 20% of the force is due to changes in enthalpy. Indeed, these $\mathbf{F}_h/\mathbf{F}$ values can be negative at low extensions, as in the case for the FL silk, and this suggests there is more than enough entropy to explain the elastic force.

The intercepts of the uncorrected, normalized force–temperature plots, $\mathbf{F}_h/\mathbf{F}$, were calculated for a number of experiments at different extensions, and the values for *Araneus* and *Nephila* MA silk are plotted in Fig. 5. It is important to note that the size of the symbols used in this plot is larger than any of the standard error bars calculated for these data. Thus, the extrapolated $\mathbf{F}_h/\mathbf{F}$ values are very precise, but the results are quite variable. In spite of this variation, the thermoelastic behaviour of these two silks is clearly different. *Nephila* MA silk is dominated by enthalpy for extensions above about 5%, whereas *Araneus* MA silk exhibits a large entropic component at all extensions. In *Nephila* MA silk an entropic component was only detected at low extensions, and the enthalpic component increased with increasing extension. Although the $\mathbf{F}_h/\mathbf{F}$ values for *Araneus* MA silk between extensions of 9% and 20% [taken from the Gosline et al. study (Gosline et al., 1984)] were negative or close to zero, there was an indication of an increase in $\mathbf{F}_h/\mathbf{F}$ with extension. Several additional measurements were made to see if this trend continued at higher extensions, and there appears to be a significant increase in $\mathbf{F}_h/\mathbf{F}$ with extension. These initial data are consistent with the hypotheses stated above, because they seem to suggest a large enthalpic contribution to the elastic mechanism of *Nephila* MA silk and a large entropic contribution to *Araneus* MA and FL silks. However, they are not conclusive because they do not account for thermal swelling changes.

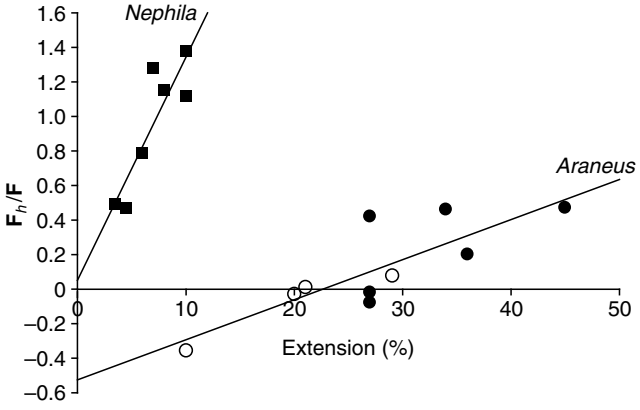

Fig. 5. Values of $\mathbf{F}_h/\mathbf{F}$ are plotted against extension for *Araneus* and *Nephila* MA silk. *Nephila* MA values are represented by black squares and are fitted to the linear regression, y=0.13x+0.51; N=7; R^2=0.77; P<0.01. Measurements on *Araneus* MA silk are represented by black circles; open circles are $\mathbf{F}_h/\mathbf{F}$ values taken from Gosline et al. (Gosline et al., 1984). The *Araneus* MA $\mathbf{F}_h/\mathbf{F}$ data are fitted to the linear regression, y=0.02x–0.53; N=10; R^2=0.68; P<0.01.

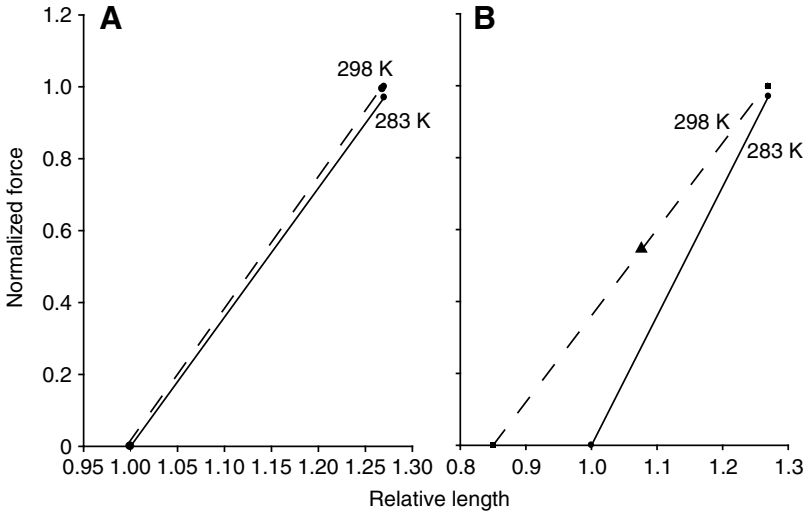

Fig. 6. Force–length isotherms are plotted to demonstrate the force correction for a typical thermoelastic test of *Araneus* MA silk at an extension of 27%. (A) The force on a fibre at a relative length of 1.27 is plotted for temperatures of 283 K (reference temperature) and at 298 K. The dashed line shows the regression between the force measured at 298 K and a relative length of 0.99, which was calculated based on the thermal swelling coefficient of 1×10^{-4} °C^{-1} for *Araneus* MA silk. Owing to the small value of the correction, the uncorrected and corrected isotherms are difficult to distinguish. (B) The force at a relative length of 1.27 is measured at 283 K (reference temperature) and at 298 K. At the reference temperature of 283 K, the relative length at zero force is 1.0 and a relative length of 1.27 is equivalent to an extension of 27%. However, with a thermal swelling coefficient of -1×10^{-2} °C^{-1}, the zero force length at 298 K is reduced to 0.85. This occurs because, at 298 K, the initial length has decreased because of a thermal de-swelling, and thus the extension of the fibre has increased. At 298 K, an extension of 27% occurs at a relative length of 1.08. The linear regression between the measured force and the zero force length (dashed line) is solved at 1.08 to determine the force at a constant extension of 27%, and is represented by the black triangle. An exaggerated thermal swelling coefficient of -1×10^{-2} °C^{-1} was chosen to better demonstrate the correction process.

Swelling

In the current study, the zero force length of MA silk was measured at ~10°C and at ~30°C, and the thermal swelling coefficient over this range was found to be -0.81×10^{-4} °C^{-1} ($\pm -0.31\times10^{-4}$ °C^{-1}; N=5) for *Araneus* MA silk. Gosline et al. (Gosline et al., 1984) measured the zero force length of *Araneus* MA silk as a function of temperature and found a linear decrease in the length of the silk between 10° and 30°C, giving a thermal swelling coefficient over this range of -1.8×10^{-4} °C^{-1} The thermal swelling coefficient of the *Nephila* MA silk was found to be -1.6×10^{-5} °C^{-1} ($\pm6.7\times10^{-5}$ °C^{-1}; N=5), and given the large error for this measurement, the coefficient could not be distinguished from zero.

Swelling correction and calculation of F_e/F

Since the thermal swelling coefficient for *Nephila* MA silk was too low to be detected, we concluded that $\mathbf{F}_h/\mathbf{F}\approx\mathbf{F}_e/\mathbf{F}$ for this silk. *Araneus* MA silk, however, required a correction because a significant thermal swelling coefficient was obtained. Swelling corrections were applied as follows. The negative thermal swelling coefficient for *Araneus* MA silk indicates that the length of an unstretched *Araneus* MA fibre decreases with increasing temperature. Thus, when a stretched fibre sample is held at constant length while the temperature is increased, the fibre extension will increase as a result of the temperature-dependent swelling. To obtain force–temperature curves at constant extension, a force–length isotherm was generated according to the following process (Shadwick and Gosline, 1985). Force–length isotherms in Fig. 6 were plotted from the regression lines generated from the force–temperature data from a typical experiment for *Araneus* MA silk at 27% extension. The force measured at this extension was plotted at the highest and lowest temperatures, and the relative lengths at zero force were plotted for each temperature based on the thermal swelling coefficient. Fig. 6A shows a plot of these points from a typical force–temperature experiment using a thermal swelling coefficient of -1×10^{-4} °C^{-1}. Owing to the small value of the swelling coefficient, the uncorrected and corrected isotherms are difficult to distinguish, and Fig. 6B shows the same data, but with an exaggerated thermal swelling coefficient of -1×10^{-2} °C^{-1}. Increasing temperature decreases the initial length of the silk, and therefore the zero force length at 298 K is shorter than that at 283 K. Thus, the silk fibre is at a larger extension at 298 K because of this swelling phenomenon. Based on the new dimensions of the silk at 298 K, the force at constant extension can be calculated. The slope of the force–temperature curve is reduced by eliminating the force increase with temperature due to the decrease in linear dimensions of the silk from solvent de-swelling. The corrected slope for *Araneus* MA silk, based on a thermal swelling coefficient of -1×10^{-4} °C^{-1}, is shown in Fig. 7. Note that the effect of the swelling correction is to raise the magnitude of the intercept; in this case, the intercept is about 0.3, or approximately 30% of the total force.

Fig. 8 shows the corrected intercepts, $\mathbf{F}_e/\mathbf{F}$, against extension for all samples of *Araneus* and *Nephila* MA silk. The *Nephila* data remain unchanged from Fig. 5 because no swelling corrections were applied, but the *Araneus* data have shifted upwards, making $\mathbf{F}_e/\mathbf{F}$ positive at all extensions. It is clear that both silks show a rise in bond-energy elasticity as they are stretched, but this rise is most dramatic in the *Nephila* silk. By an extension of about 10% the bond-energy component of the force is actually greater than 1, indicating that bond-energy elasticity can account for all of the elastic force. *Araneus*, however, shows a more gradual rise in $\mathbf{F}_e/\mathbf{F}$, from about 0.1 at the lowest stresses to about 0.5 at 50% extension.

It was expected that the aqueous, glue-coated FL silk would exhibit entropic elasticity because of its low initial stiffness and long-range elasticity. Fig. 9 shows $\mathbf{F}_h/\mathbf{F}$ and $\mathbf{F}_e/\mathbf{F}$ plotted against extension for *Araneus* FL silk. The $\mathbf{F}_h/\mathbf{F}$ values are negative at all extensions tested. Unfortunately, it was not possible to measure the thermal swelling coefficient for FL silk because of the short lengths of the available fibres; however, the swelling was assumed to be larger than the swelling for MA silk, and a value of -4×10^{-4} °C^{-1} was chosen. In most cases, this correction created a $\mathbf{F}_e/\mathbf{F}$ value at or close to zero, and there was no significant slope to these data. However, in five experiments at low extensions $\mathbf{F}_h/\mathbf{F}$ is exceptionally negative, and a thermal swelling coefficient of -4×10^{-4} °C^{-1} was clearly not sufficient to create a near zero or positive $\mathbf{F}_e/\mathbf{F}$. In Fig. 9, these outliers with $\mathbf{F}_h/\mathbf{F}$ <–1.0 obscure the trend about zero, and in Fig. 10 the data are re-plotted with the outliers removed on an expanded normalized-force axis. The removal of outliers suggests that $\mathbf{F}_e/\mathbf{F}$ does not show an increasing trend with extension up to 100%.

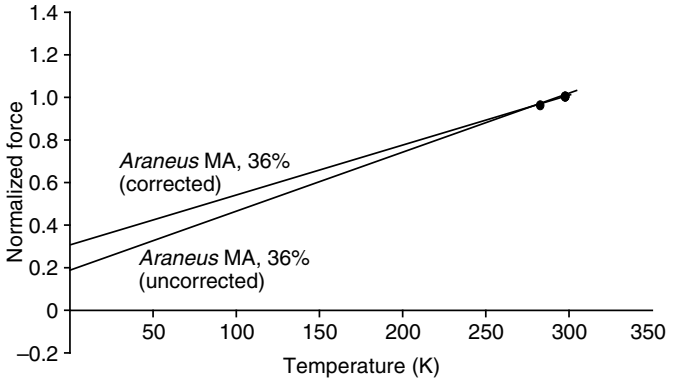

Fig. 7. A plot of normalized force against temperature for a sample of *Araneus* MA silk held at an extension of 36%. The intercept of the uncorrected plot is 0.2, indicating that for this sample approximately 20% of the force is due to enthalpy. When corrected for the effects of thermal swelling, the slope of the force–temperature plot decreases, and the intercept rises to 0.30 for this silk sample, indicating that approximately 30% of the force is due to bond energy.

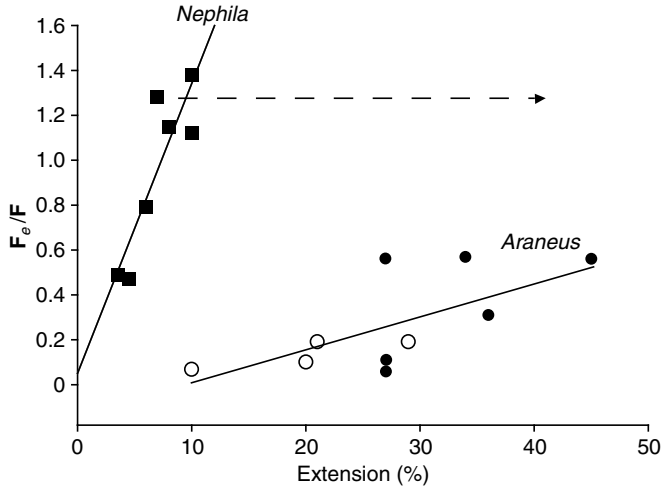

Fig. 8. Values of $\mathbf{F}_e/\mathbf{F}$ are plotted against extension for *Araneus* and *Nephila* MA silk. No swelling correction was applied to *Nephila* MA silk and so the $\mathbf{F}_h/\mathbf{F}$ values (Fig. 5) are equivalent to $\mathbf{F}_e/\mathbf{F}$. *Nephila* MA silk values are represented by black squares and are fitted to the linear regression, y=0.13x+0.51; N=7; R^2=0.77; P<0.01. *Araneus* MA silk measurements are represented by black circles; open circles are $\mathbf{F}_e/\mathbf{F}$ values taken from Gosline et al. (Gosline et al., 1984). The *Araneus* MA $\mathbf{F}_e/\mathbf{F}$ data are fitted to the linear regression, y=0.02x–0.15; N=10; R^2=0.68; P<0.01.

DISCUSSION

The thermoelastic experiments presented in this study are entirely consistent with the conclusion of our previous paper (Savage and Gosline, 2008), that the presence of proline in the glycine-rich network chains plays a key role in determining the structure of the fibroin networks in MA silks. *Araneus diadematus* MA glands are unique among those studied thus far, in having two spidroin-2 type genes expressed (Guerette et al., 1996). A spidroin-1 type fibroin is present in the *Araneus* genome (Gatsey et al., 2001), but was found to be expressed only in the cylindrical gland and was below detection limits in the MA gland (Guerette et al., 1996). Thus, the predominant fibroins expressed in the *Araneus* MA gland contain about 16% proline, and this silk contains amorphous network chains and exhibits rubber-like elasticity when hydrated. By contrast, *Nephila* MA silk, which contains primarily spidroin-1 fibroins and has low proline content, has semi-ordered network chains and exhibits bond-energy elasticity when hydrated.

The uncorrected thermodynamics (Fig. 5) indicate that the enthalpic component of the elastic force, $\mathbf{F}_h/\mathbf{F}$, is small in *Araneus* MA silk. Indeed $\mathbf{F}_h/\mathbf{F}$ is negative in some samples, which suggests that the entropic component is more than sufficient to account for the elasticity of this material. The situation is dramatically different for *Nephila* MA silk. The enthalpic component of the elastic force is dominant at all extensions, and an entropic component of the elastic force is only seen at the smallest extensions. Thus, it appears that hydrated *Araneus* MA silk contains a network of kinetically-free protein chains and is truly an entropic rubber. By contrast, hydrated *Nephila* MA silk exhibits bond-energy elasticity associated with the presence of stable secondary structures within its network chains. However, before we accept these conclusions, it is important to consider the thermal swelling and its effect on the thermodynamics of these systems.

Our estimate of the thermal swelling coefficient for *Araneus* MA silk, -1×10^{-4} °C^{-1}, is similar to that recorded previously (Gosline et al., 1984) and allowed us to estimate the bond-energy component of the elastic force, $\mathbf{F}_e/\mathbf{F}$, which turned out to be very small, particularly at small extensions (Fig. 8). Hence, our data are entirely consistent with the interpretation that hydrated *Araneus* MA silk is an entropic rubber. Our attempts to measure the thermal swelling coefficient for *Nephila* were largely unsuccessful because our method was not precise enough to actually quantify the swelling of this material. The uncertainty of our measurement, -1.6×10^{-5} °C^{-1} ($\pm6.7\times10^{-5}$ °C^{-1}), is so large relative to the mean that we cannot even determine if the coefficient is positive or negative. We chose, therefore, to treat the coefficient as zero, and we present the $\mathbf{F}_h/\mathbf{F}$ as giving a best estimate of the bond-energy component of the elastic force $\mathbf{F}_e/\mathbf{F}$. The data for *Nephila* MA silk in Figs 5 and 7 suggest that by an extension of 10%, $\mathbf{F}_e/\mathbf{F}$=1.4, meaning that there is 40% more bond-energy available than is needed to account for the elastic force. This is almost certainly not true, and it leads to the conclusion that if we could measure the thermal swelling coefficient of hydrated *Nephila* MA silk, it would likely be positive and have a magnitude of approximately $+3\times10^{-5}$ °C^{-1}. That is, this level of positive swelling would be just sufficient to shift the highest $\mathbf{F}_h/\mathbf{F}$ to an $\mathbf{F}_e/\mathbf{F}$ value of 1.0, indicating that all of the elastic force at 10% extension is due to bond-energy elasticity. It remains to be seen if this is true.

Interestingly, it is not necessarily true that an improved method would actually improve the precision of this experiment. Recall that, from the previous study of the mechanical and optical properties of hydrated *Araneus* and *Nephila* MA silks, these silks are highly variable in their properties [see Figs 4–7 in Savage and Gosline (Savage and Gosline, 2008)]. Thus, the variation in the thermal swelling coefficient is likely to arise from sample variation as opposed to measurement error. To truly resolve this issue with *Nephila* silk, it may be necessary to conduct thermoelastic experiments and measure the thermal swelling coefficient on the same sample, which we were unable to do in this study.

One interesting feature of the thermoelasticity of both MA silks is that the bond-energy component of the elastic force, $\mathbf{F}_e/\mathbf{F}$, seemed to increase with extension, a feature not usually seen for lightly cross-linked natural rubbers, or for the protein rubbers elastin and resilin. This very likely reflects the presence of crystalline structures in the networks of the MA silks, which become more prominent as extension proceeds. By contrast, natural rubber, resilin and elastin are crosslinked covalently by structures that are much smaller than

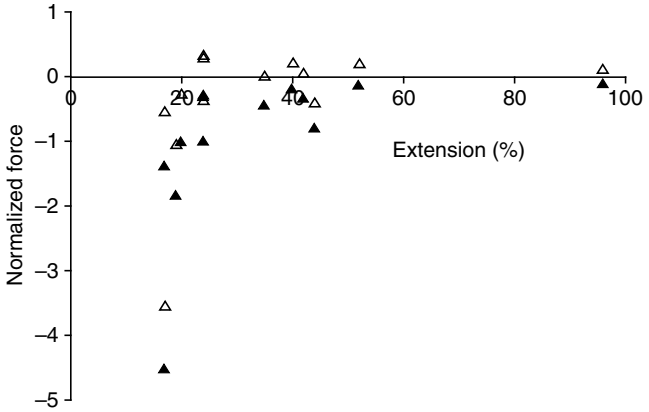

Fig. 9. Values of $\mathbf{F}_h/\mathbf{F}$ (black triangles) and $\mathbf{F}_e/\mathbf{F}$ (open triangles) for *Araneus* FL silk are plotted against extension. Note that the $\mathbf{F}_h/\mathbf{F}$ values are negative at all extensions tested.

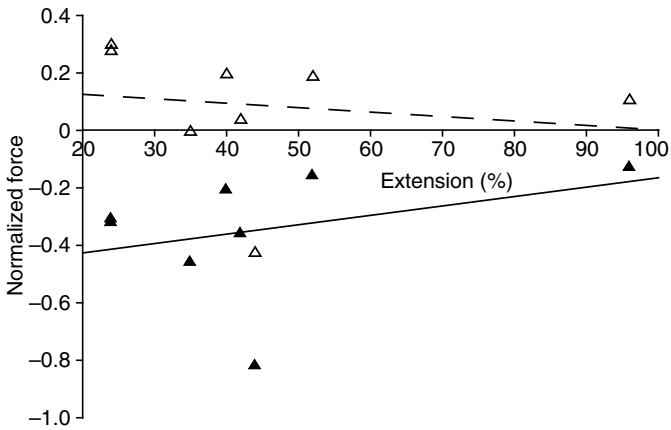

Fig. 10. The *Araneus* FL silk values for $\mathbf{F}_h/\mathbf{F}$ (black triangles) and $\mathbf{F}_e/\mathbf{F}$ (open triangles) from Fig. 8 are plotted against extension. The most negative outliers from Fig. 8 have been omitted in order to better view the trend about zero on the force axis. The values of $\mathbf{F}_h/\mathbf{F}$ and $\mathbf{F}_e/\mathbf{F}$ have each been fitted to a linear regression; neither regression has a slope significantly different from zero.

the β-sheet crystals that crosslink and reinforce the networks in the spider MA silks. We therefore carried out our thermoelastic experiments over a range of extensions to evaluate the extent of this shift from entropic to bond-energy elasticity. The trends for the MA silks are clear, but there is considerable scatter because of the enormous variation seen in the structure and properties of these silks (Savage and Gosline, 2008).

In the case of *Araneus* MA, there was a modest rise in the bond-energy component of the elastic force at extensions above about 20%, and by 50% extension $\mathbf{F}_e/\mathbf{F}\approx0.5$. This rise may indicate that the relatively large, poly-alanine, β-sheet crystals are constraining the network chains in a way that causes this rise in bond-energy elasticity at higher extensions. Indeed, Termonia (Termonia, 1994) developed a model for the structure and mechanical properties of MA silks that was based on the thermoelastic properties of hydrated *Araneus* MA silk (Gosline et al., 1984). That is, he assumed that the glycine-rich network chains were amorphous and behaved as kinetically-free random-coils in the hydrated state. He found that it was only possible to predict the properties for wet and dry MA silk if he included a layer of greater stiffness in the network chains just outside the β-sheet crystals. He assumed a 5 nm thick layer with a sixfold increase in stiffness, and his model successfully predicted the stress–strain properties of both hydrated and dry *Araneus* MA silk. This layer of increased stiffness was attributed to the physical constraint of network chains emerging from the β-sheet crystals in dense clusters, and hence with restricted mobility. The rise in $\mathbf{F}_e/\mathbf{F}$ between 20% and 50% extension probably reflects a rising contribution to the elasticity of hydrated *Araneus* MA silk from the deformation of these conformationally constrained regions of the network chains.

The situation for *Nephila* MA silk is clearly quite different. $\mathbf{F}_e/\mathbf{F}\approx0.5$ at 5% extension, and it rises rapidly to essentially 1 by 10% extension. This clearly indicates a much more dominant role for bond-energy elasticity in the *Nephila* silk. Thus, it is appropriate to conclude that stable, secondary structures are present in the network chains of *Nephila* MA silk, and that entropic processes are only important at very low extensions where these secondary structures reorient before they are actually strained. By about 10% extension, therefore, the deformation of stable secondary structures becomes the dominant feature of this silk. The dashed arrow in Fig. 8 indicates the trend that we would expect to see for *Nephila* silk at higher extensions, namely that bond-energy elasticity will be maintained at this high level. Unfortunately, we could not confirm this because the stiffness of the silk was so great at higher extensions that we could not carry out thermoelastic tests with the apparatus we had constructed.

The experiments with *Araneus* FL silk reinforces the conclusion that proline plays a key role in creating a network of kinetically-free, amorphous chains in hydrated spider silks. The thermoelastic data in Figs 9 and 10 clearly indicate that changes in conformational entropy are responsible for the storage of elastic energy in this silk. Most values of $\mathbf{F}_h/\mathbf{F}$ were close to zero or slightly negative, and the application of a thermal swelling coefficient of -4×10^{-4}°C^{-1} brings the predicted $\mathbf{F}_e/\mathbf{F}$ values into full agreement with a conformational entropy system. It is important to note that this swelling coefficient is just a guess, and the validity of this conclusion rides on the reasonableness of the guess. We assumed that the thermal swelling coefficient for FL silk would be negative, like that of *Araneus* MA silk, because the glycine-rich chains in both silks are very similar, both in the relative contents of glycine and proline and in the arrangement of these and the other residues. Based on this assumption, there are two good reasons why the magnitude of the thermal swelling coefficient for FL silk should be larger than that for MA silk.

First, *Araneus* FL silk network chains are much longer (~115 residues) than those in *Araneus* MA silk (~25 residues), which means that the stiffness of FL silk will be lower. This is actually true, as supercontracted *Araneus* MA silk has an average initial stiffness of 10 MPa (Gosline et al., 1994; Savage and Gosline, 2008), and water-swollen *Araneus* FL silk has an average initial stiffness of 1 MPa (Pollak, 1991; Gosline et al., 1994). Thus, temperature effects on the chain chemistry should have a much larger effect on the swollen volume of the softer network, as predicted by the Flory–Rehner Theory for network swelling (Flory, 1953).

In addition, the MA silk has a higher content of β-sheet crystals, again because of its sequence design, and when the MA silk supercontracts, the abundant crystals and short network chains prevent the material from relaxing to a completely isotropic state. Thus, supercontracted *Araneus* MA silk has a birefringence of 6×10^{-3}, which indicates some residual orientation of crystals parallel to the fibre axis. Hydrated *Araneus* FL silk has a

birefringence of 9×10^{-4} (Gosline et al., 1995), and this sevenfold lower birefringence indicates that the properties of FL silk are more nearly isotropic than those of the MA silk. Thus, even if thermal changes in swelling cause equal increases the volumes of the two silks, the FL silk will expand more along its fibre axis, giving it a higher thermal swelling coefficient. Thus, our guess of -4×10^{-4}°C^{-1} for the thermal swelling coefficient is reasonable, if not exact.

Interestingly, five of the FL samples had extremely negative $\mathbf{F}_h/\mathbf{F}$ values that remained large and negative after correction for swelling. This is not surprising, given the extreme variability that has been observed for the mechanical properties of hydrated FL silks (Pollak, 1991; Gosline et al., 1994). This variation in mechanical properties would lead to variation in swelling behaviour, and it is not surprising that some samples could not be adequately corrected with a single, assumed value for the thermal swelling coefficient. As with the results for *Nephila* MA silk, if we were able to measure the thermal swelling coefficient of each sample subjected to thermoelastic analysis, we would discover that these exceptional samples would show the same behaviour as indicated in Fig. 10 for the majority of FL silk samples.

The structural state of the network chains in MA and FL silks

Our results show that the glycine-rich network chains are very different in *Araneus* and *Nephila* MA silks, and we believe that this difference is due to the difference in proline levels in the fibroins that make up these two silks. Proline is known to disrupt secondary structure in glycine-rich peptide sequences (Rauscher et al., 2006), and the high levels of proline in the network chains of *Araneus* MA silk are almost certainly responsible for the mobility of the network chains in hydrated *Araneus* MA silk. Interestingly, amino acid sequences from this silk indicate that the majority of network chains contain a proline within three to five residues upon exiting β-sheet crystals. Presumably, the effect of this proline is to increase flexibility and loosen the constrained clusters as the chains emerge from the β-sheet crystals. Although we believe that the thermoelastic data presented here provide the strongest demonstration of the amorphous and kinetically-free structure of the network chains in *Araneus* MA silk, Shao et al. (Shao et al., 1999) used single-fibre Raman spectroscopy to probe the effect of solvent on its structure, and these data provide additional evidence to support this conclusion. Differences between the Raman spectra taken parallel to and perpendicular to the fibre reveal a high degree of order in dry *Araneus* MA silk, a finding that is consistent with a spinning process that would orient the β-sheet crystals and all or most of the network chains in the dry fibre. However, this study could not quantify the conformational components that would indicate what, if any, secondary structure stabilized this alignment in the network chains of the dry thread. With supercontraction, the peaks in the Raman spectra associated with random-coil and β-sheet, increased and decreased, respectively, upon supercontraction. The spectra indicated that the β-sheets remain in the supercontracted state but lose much of their alignment, while the network chains appear to become random-coils.

The situation for *Nephila* MA silk is very different. The dominance of bond-energy elasticity in this silk in its hydrated state clearly suggests the presence of stable secondary structures in the glycine-rich network chains, and the prevalence of the proline-free spidroin-1 in this silk suggests that the lack of proline may enable this structure. Although the thermoelastic evidence presented here is consistent with this conclusion, it does not provide information to distinguish between the secondary structures that have been proposed for the glycine-rich sequences in *Nephila* MA silk. Thus, it remains to be determined if the non-periodic lattice β-sheet crystal structure (Thiel et al., 1997) or the 3_1 helix structure (Kümmerlen et al., 1996; van Beek et al., 2002) is most appropriate. Either should be quite rigid and could explain the bond-energy nature of the elastic mechanism in *Nephila* MA silk. That is, as the fibre is stretched, the inter-chain hydrogen bonds in these ordered regions are deformed and could play a major role in the elastic recoil of the fibre. More recently Eles and Michal (Eles and Michal, 2004a) have shown through NMR of glycine-labelled, dry *Nephila* MA silk that 47% of glycines are well oriented to the fibre axis and 53% are poorly oriented (Eles and Michal, 2004a). They concluded that the orientation of ordered glycine-rich network chains is consistent with 3_1 helices, but this is not direct evidence for the presence of such structure. Eles and Michal (Eles and Michal, 2004b) used NMR to probe the network structure of dry, hydrated but partially restrained, and fully supercontracted *Nephila* MA silk. Again, the network chains in dry *Nephila* MA silk are in highly extended conformations; however, these chains became more mobile as the hydrated silk was allowed to shorten. The authors concluded that network chains acted as entropic springs in supercontracted silk and that the molecular mechanism of the dry silk was based on "latent entropic springs" that are axially aligned by the spinning process and stabilized by hydrogen bonding in the absence of water.

In summary, our thermoelastic analysis of the MA and FL silks from *Araneus diadematus* and the MA silk *Nephila clavipes* confirm the conclusion of our previous study that proline residues present in the glycine-rich network chains of spider silk fibroin networks will destabilize secondary structures and will favour a more amorphous network structure. This leads to an entirely new avenue of enquiry into the functional significance of proline-rich and proline-deficient fibroin networks. We suspect that the difference in fibroin expression levels between species may reflect differences in the physical environment in which these species live, allowing them to adjust material properties to suit the key function or functions of their MA silks. In addition, it will be interesting to see if changes in fibroin expression occur during ontogeny or with environmental changes. There is clearly much left to learn about the interface between the polymer physics and mechanics of spider silks and the biology of these amazing animals.

This study was supported by Grant 6934-04 from the Natural Sciences and Engineering Research Council of Canada to J.M.G.

REFERENCES

Alexander, R. M. (1966). Rubber-like properties of the inner hinge ligament of Pectinidae. *J. Exp. Biol.* **44**, 119-130.

Dorrington, K. L. and McCrum, N. G. (1977). Elastin as a rubber. *Biopolymers* **16**, 1201-1222.

Eles, P. T. and Michal, C. A. (2004a). A DECODER NMR study of backbone orientation in *Nephila* clavipes dragline silk under varying strain and draw rate. *Biomacromolecules* **5**, 661-665.

Eles, P. T. and Michal, C. A. (2004b). Strain dependent local phase transitions observed during controlled supercontraction reveal mechanisms in spider silk. *Macromolecules* **37**, 1342-1345.

Flory, P. J. (1953). *Principles of Polymer Chemistry*. London: Cornell University Press.

Fudge, D., Gardner, K. H., Forsyth, V. T., Riekel, C. and Gosline, J. (2003). The mechanical properties of hydrated intermediate filaments: Insights from hagfish slime threads. *Biophys. J.* **85**, 2015-2027.

Gatesy, J., Hayashi, C., Motriuk, D., Woods, J. and Lewis, R. (2001). Extreme diversity, conservation, and convergence of spider silk fibroin sequences. *Science* **291**, 2603-2605.

Gosline, J. M. (1980). The elastic properties of rubber-like proteins and highly extensible tissues. *Symp. Soc. Exp. Biol.* **34**, 332-357.

Gosline, J. M., Denny, M. W. and Edwin, D. M. (1984). Spider silk as rubber. *Nature* **309**, 551-552.

Gosline, J. M., Pollak, C. C., Guerette, P. A., Cheng, A., DeMont, M. E. and Denny, M. W. (1994). Elastomeric network models for the frame and viscid silks from the orb web of the spider *Araneus diadematus*. In *Silk Polymers, Materials Science and Biotechnology* (ed. D. Kaplan, W. Adams, B. Farmer and C. Viney), pp. 328-341. Washington, DC: American Chemical Society.

Gosline, J., Nichols, C., Guerette, P., Cheng, A. and Katz, S. (1995). The macromolecular design of spiders' silks. In *Biomimetics: Design and Processing of Materials* (ed. M. Sarikaya and I. A. Aksay), pp. 236-261. Woodbury, NY: American Institute of Physics.

Guerette, P., Ginzinger, D., Weber, B. and Gosline, J. M. (1996). The spider silk fibroin gene family: gland specific expression controls silk properties. *Science* **272**, 112-115.

Kümmerlen, J., van Beek, J. D., Vollrath, F. and Meier, B. H. (1996). Local structure in spider dragline silk investigated by two-dimensional spin-diffusion nuclear magnetic resonance. *Macromolecules* **29**, 2920-2928.

Pollak, C. C. (1991). Mechanical and optical analyses provide a network model for spiral silk from the orb web of the spider *Araneus diadematus*. MSc. Thesis. Department of Zoology. Vancouver, BC, Canada: University of British Columbia.

Rauscher, S., Baud, S., Miao, M., Keeley, F. W. and Pomes, R. (2006). Proline and glycine control protein self-organization into elastomeric or amyloid fibrils. *Structure* **14**, 1667-1676.

Savage, K. N. and Gosline, J. M. (2008). The effect of proline on the network structure of majoe ampullate silks as inferred from their mechanical and optical properties. *J. Exp. Biol.* **211**, 1937-1947.

Savage, K. N., Guerette, P. A. and Gosline, J. M. (2004). Supercontraction stress in spider webs. *Biomacromolecules* **5**, 675-679.

Shadwick, R. E. and Gosline, J. M. (1985). Physical and chemical properties of rubber-like elastic fibres from the octopus aorta. *J. Exp. Biol.* **114**, 239-257.

Shao, Z. R., Young, R. J. and Vollrath, F. (1999). The effect of solvents on spider silk studied by mechanical testing and single-fibre Raman spectroscopy. *Int. J. Biol. Macromol.* **24**, 295-300.

Termonia, Y. (1994). Molecular modeling of spider silk elasticity. *Macromolecules* **27**, 7378-7381.

Thiel, B. L., Guess, K. B. and Viney, C. (1997). Non-periodic lattice crystals in the hierarchical microstructure of spider (major ampullate) silk. *Biopolymers* **41**, 703-719.

Treloar, L. R. G. (1975). *The Physics of Rubber Elasticity* (3rd edn). Oxford: Clarendon Press.

van Beek, J. D., Hess, S., Vollrath, F. and Meier, B. H. (2002). The molecular structure of spider dragline silk: folding and orientation of the protein backbone. *Proc. Natl. Acad. Sci. USA* **99**, 10266-10271.

Weis-Fogh, T. (1961). Thermodynamic properties of resilin, a rubber-like protein. *J. Mol. Biol.* **3**, 520-531.